

## Resonance Raman scattering in HgTe: TO-phonon and forbidden-LO-phonon cross section near the $E_1$ gap

Alka Ingale, M. L. Bansal, and A. P. Roy

*Nuclear Physics Division, Bhabha Atomic Research Centre, Trombay, Bombay 400 085, India*

(Received 25 August 1989)

In this paper we present Raman intensity variation of the TO phonon and the forbidden LO phonon in HgTe. We evaluate the optical-phonon deformation potentials near the  $E_1$  gap ( $d_{10}^5 = 24$  eV and  $d_{30}^5 = 20$  eV). The differences that arise as a consequence of the inverted band structure of HgTe are discussed and it is shown that the standard macroscopic formalism for Raman susceptibility for the TO-phonon mode in terms of linear susceptibility can be applied to HgTe also. Investigation of forbidden-LO-phonon intensity reveals that impurity-induced scattering is dominant and interband electron-phonon scattering has to be explicitly included to account for its variation with laser wavelength.

### I. INTRODUCTION

The resonance enhancement of the Raman cross section in the vicinity of the interband critical points ( $E_0$ ,  $E_1$ , and their spin-orbit-split counterparts) has been investigated in Ge, Si, and several zinc-blende compound semiconductors.<sup>1,2</sup> Variation of the cross section in the neighborhood of electronic critical points provides important information about the electron-phonon interaction. Specifically one can obtain information about the phonon-induced modulation of band gaps (two-band process) and the phonon-induced mixing of the wave functions of the two spin-orbit-split bands (three-band processes).

Zero-band-gap semiconductors (semimetals) such as HgTe, HgSe, etc., have simple zinc-blende crystal structure with inverted band gap.<sup>3</sup> Their electronic band structure is quite similar (apart from being inverted) to other zinc-blende compounds such as InSb, GaAs, etc., with the important difference that the two valence bands originate from  $p$ - and  $s$ -like atomic states and are not spin-orbit-split partners. However, Raman scattering investigations from these systems have been rather limited.<sup>4-6</sup> In this paper we present variation of the Raman cross section for the TO phonon and "forbidden" LO phonon in HgTe as a function of incident laser energy near the  $E_1$  and  $E_1 + \Delta_1$  gaps. The main aim of the work was to see whether any phonon-induced mixing of the two valence bands contributes to Raman scattering. We find that the contribution is quite significant and modifies the shape of the Raman resonance curve significantly.

The outline of the paper is as follows. In Sec. II the general theory for allowed scattering is discussed. HgTe has "inverted band structure" and therefore formulas written in Sec. II have to be applied with caution. Section III deals with the measurement of linear susceptibility and its implications. In Sec. IV we give details of experimental setup. Section V discusses resonance behavior for allowed TO phonon and forbidden LO phonon, re-

spectively. Finally main conclusions are summarized in Sec. VI.

### II. THEORY

The photon counting rate outside the sample is given by<sup>1,2</sup>

$$\mathcal{S}^* = \left[ \frac{T_S T_L}{(\alpha_L + \alpha_S) \eta_L \eta_S} \right] \frac{N \omega_S^3 P_L [\eta(\Omega_{\text{ph}}) + 1]}{2M^* \Omega_{\text{ph}} C^4} \times \Delta\Omega' |\hat{\mathbf{e}}_S \cdot \vec{\mathcal{R}} \cdot \mathbf{e}_L|^2, \quad (1)$$

where  $P_L$  is the incident laser power,  $T_{S,L} = 1 - R_{S,L}$  is the fraction transmitted across the sample interface for the scattered ( $\omega_S$ ) or incident ( $\omega_L$ ) photons. The factor  $\Delta\Omega' / \eta_S^2$  is the collection angle inside the sample, with  $\eta_S / \eta_L$  accounting for effective energy densities inside the sample.  $N$  is the number of unit cells per unit volume.  $\eta(\Omega_{\text{ph}})$  is the Bose-Einstein factor for phonon of frequency  $\Omega_{\text{ph}}$ .  $M^*$  is the reduced mass  $[= M_{\text{Hg}} M_{\text{Te}} / (M_{\text{Hg}} + M_{\text{Te}})]$  for the optic phonon under consideration in HgTe.

The actual counting rate in an experiment will differ from that given by Eq. (1) by a factor depending upon the spectrometer throughput and detector efficiency. To evaluate this factor as a function of  $\omega_L$ , a known standard such as Si, CaF<sub>2</sub>, diamond, etc., is used.

The last factor in Eq. (1), i.e.  $|\hat{\mathbf{e}}_S \cdot \vec{\mathcal{R}} \cdot \mathbf{e}_L|$  is the Raman polarizability associated with the particular phonon and contracted with incident and scattered polarizations. The independent components of  $\vec{\mathcal{R}}$  are called Raman polarizabilities. HgTe with zinc-blende structure has only one independent Raman polarizability component denoted by  $a$  and  $\mathcal{R}_{ij} = (1 - \delta_{ij})a$ .

It is the variation of  $a$  which is measured experimentally. The frequency dependence of the Raman polarizability  $a$  near the interband critical points  $E_1$  and  $E_1 + \Delta_1$  is given by<sup>2</sup>

$$a_{\text{TO}}(E) = \frac{a_0^2}{4\sqrt{6}} \left[ \frac{1}{2\sqrt{2}} d_{10}^5 \frac{d\chi(E)}{dE_1} + 2d_{30}^5 \frac{\chi^{E_1}(E) - \chi^{E_1+\Delta_1}(E)}{\Delta_1} + C \right] \quad (2)$$

where  $a_0$  is the lattice constant. The first term in the large parentheses arises from two-band processes produced by the phonon-induced modulation of the  $E_1$  gap, the deformation potential  $d_{10}^5$  representing the change in  $E_1$  per unit phonon displacement. The mixing of the two spin-orbit-split valence bands via the phonon produces the second term in Eq. (2). The strength of this coupling is given by the deformation potential  $d_{30}^5$ . Microscopic derivation of the three-band term in this equation assumes near equality of transition-matrix elements between the conduction band and the two valence bands.<sup>1</sup> This assumption is valid for normal zinc-blende materials but need not be valid for HgTe because of its inverted gap. We shall later comment about the applicability of this equation to HgTe.

Now we come to the constant  $C$ . This essentially represents the constant contribution due to other electronic transitions of the medium; assumed far away from  $E_1$  and  $E_1 + \Delta_1$ . Explicitly one can write  $C$  as

$$C = \sum_{i(\neq 1)} \frac{d\chi(E)}{dE_i} d_{i0}^5. \quad (3)$$

If all the other gaps,  $E_i$ 's, are far removed from  $E_1$  and  $E_1 + \Delta_1$  their contributions to  $\chi$  in the region of interest ( $E_1, E_1 + \Delta_1$  range) is linear with energy. This results in  $d\chi/dE_1$  being constant. Usually if the experimental Raman susceptibility is available over an extended range (beyond  $E_1$  and  $E_1 + \Delta_1$ ), constant  $C$  can be evaluated by treating it as an adjustable parameter. We will see in the next section that in HgTe only the  $E_2$  critical point gives small contribution to total linear susceptibility  $\chi$  in the energy range of  $E_1$  and  $E_1 + \Delta_1$ . Thus only one term in Eq. (3) needs to be considered.

### III. BAND STRUCTURE AND LINEAR SUSCEPTIBILITY FOR HgTe

The II-VI compound HgTe is semimetallic and has the so-called inverted band structure *vis-à-vis* other zinc-blende semiconductors such as InSb, CdTe etc.<sup>3</sup> The band structure of interest is shown in Fig. 1. Here the conduction band is a consequence of crystal-field (s.o.) splitting of a  $p$ -like state, whereas in GaAs, etc. it originates from a  $s$ -like state. In HgTe the heavy-hole (hh, upper) valence band is a consequence of a split  $p$ -like state whereas the light-hole (lh, lower) valence band originates from  $s$ -like state. In InSb the lower two valence bands are a consequence of crystal-field splitting of  $p$ -like states. However, the symmetry irreducible representation of the conduction ( $L_6$ ), hh valence ( $L_{4,5}$ ) and lh valence ( $L_6$ ) bands at the  $L$  point remains the same as that in InSb. The quantities  $E_1$  and  $E_1 + \Delta_1$  in HgTe are quite similar to that in InSb ( $E_1 \sim 1.98$  eV,  $\Delta_1 \sim 0.5$  eV for InSb and  $E_1 = 2.1$  eV and  $\Delta_1 \sim 0.6$  for HgTe).

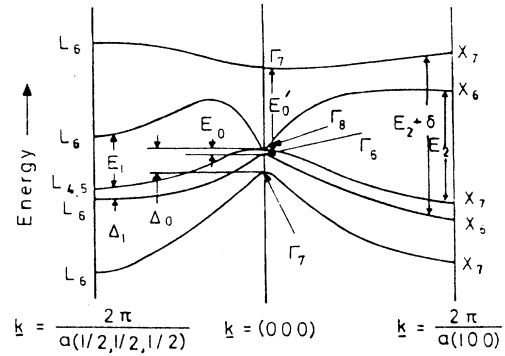


FIG. 1. Electronic band structure of HgTe. Notice the origin of the two valence bands ( $L_{4,5}$  and  $L_6$ ).

Ellipsometric measurements on HgTe have been performed by Viña *et al.*<sup>7</sup> However, as it is clear from Eq. (1) and also shown in Ref. 8 the susceptibility  $\chi$  must be known accurately in order to obtain a reliable estimate of the Raman cross section. We have performed ellipsometric measurements on the sample of HgTe that was used for Raman spectroscopy. Following Viña *et al.*<sup>7</sup> the experimentally obtained susceptibility can be fitted assuming the  $E_1$  and  $E_1 + \Delta_1$  gaps as two-dimensional saddle points with a slight admixture of  $2d$  maxima.<sup>7,9</sup>

$$\begin{aligned} \chi^{E_1} &= -iA^{E_1} \ln(1-x)e^{i\phi_1}, \\ \chi^{E_1+\Delta_1} &= -iA^{E_1+\Delta_1} \ln(1-x')e^{i\phi_2}, \end{aligned} \quad (4a)$$

where

$$x = E/(E_1 - i\Gamma_1) \quad \text{and} \quad x' = E/(E_1 + \Delta_1 - i\Gamma_2)$$

$$\chi^{\text{total}} = \chi^{E_1} + \chi^{E_1+\Delta_1} + CE + K, \quad (4b)$$

where  $CE$  and  $K$  represent the linear and constant contributions to susceptibility, mainly due to the higher lying  $E_2$  gap. In Table I we give values of various parameters obtained through fitting of  $\chi$ .

The amplitude  $A^{E_1}$  and  $A^{E_1+\Delta_1}$ , which are functions

TABLE I. Fitted parameters for the experimental susceptibility. Parameters reproduced here in column 3 are read from curves in Ref. 7 except for  $E_1$  and  $E_1 + \Delta_1$ .

	Our measurements	Viña's measurements
$E_1$	2.15 meV	2.147 meV
$E_1 + \Delta_1$	2.75 meV	2.778 meV
$\Gamma_1$	0.09 meV	0.075 meV
$\Gamma_2$	0.12 meV	0.122 meV
$\phi_1$	0.1 rad	0.199 rad
$\phi_2$	0.2 rad	0.342 rad
$A^{E_1}$	0.18	
$A^{E_1+\Delta_1}$	0.127	

of reduced joint density of state mass ( $\mu_1^*$ ) and the momentum matrix element  $P$ , can be written explicitly as<sup>1</sup>

$$A^{E_1} = \frac{\sqrt{3}e^2}{3\pi m_0^2 a_0} \frac{|\langle c|P|hh\rangle|^2}{E^2} \mu_1^*(hh,c), \quad (5a)$$

$$A^{E_1+\Delta_1} = \frac{\sqrt{3}e^2}{3\pi m_0^2 a_0} \frac{|\langle c|P|lh\rangle|^2}{E^2} \mu_1^*(lh,c). \quad (5b)$$

Since fitting to the susceptibility data does not indicate any explicit dependence of  $A$ 's on photon energy  $E$ , the  $E^2$  terms in the denominators of Eqs. (5a) and (5b) are replaced by  $E_1^2$  and  $(E_1 + \Delta_1)^2$  respectively, as is the case for Ge.<sup>10</sup> Dividing (5a) by (5b) we have

$$\frac{A^{E_1}}{A^{E_1+\Delta_1}} = \frac{|\langle c|P|hh\rangle|^2 \mu_1^*(hh,c) (E_1 + \Delta_1)^2}{|\langle c|P|lh\rangle|^2 \mu_1^*(lh,c) E_1^2}.$$

Substituting for  $A^{E_1}$  and  $A^{E_1+\Delta_1}$  from the table along with the values of  $E_1$  and  $\Delta_1$  we obtain

$$\frac{|\langle c|P|hh\rangle|^2 \mu_1^*(hh,c)}{|\langle c|P|lh\rangle|^2 \mu_1^*(lh,c)} \simeq 0.86.$$

Within the  $\mathbf{k}\cdot\mathbf{p}$  approximation  $\mu_1^*(lh,c)$  is slightly greater than  $\mu_1^*(hh,c)$  [under the assumption of equal momentum matrix elements these masses are proportional to  $(E_1 + \Delta_1/3)$  and  $(E_1 + 2\Delta_1/3)$ , respectively]<sup>11</sup>, therefore the two transition-matrix elements connecting the two valence bands to the conduction band turn out to be nearly equal. It may be mentioned here that a similar conclusion has been arrived at earlier by a consideration of galvanomagnetic properties of HgTe.<sup>12</sup> This "equality" of momentum matrix elements implies that Eq. (2) can be used for calculating Raman susceptibility<sup>1</sup> in spite of the inverted band structure of HgTe at the  $\Gamma$  point.

In HgTe the conduction and valence bands intersect near the  $\Gamma$  point. This results in interband and intraband (single-particle and collective) electronic excitations overlapping in energy with the TO phonon. In general this type of situation can result in the Fano type of line shapes due to interference between the photons scattered due to the electronic continuum and discrete phononlike excitations.<sup>13</sup> However, when one is considering scattering near the  $E_1$  gap, the  $e$ - $h$  pair produced in the resonant scattering process is separated by a large  $q$  from the interband electronic excitations at the  $\Gamma$  point and therefore cannot excite these. Thus interference is unlikely; even though the continuum of electronic transitions can manifest itself through additional phonon damping in HgTe.

Thus despite several apparent complications in HgTe the standard formalism for scattering susceptibility [Eq. (2)] can be used.

#### IV. EXPERIMENT

Thin  $p$ -type HgTe samples ( $\sim 0.5$  mm thick) cut with a (111) face after a fine mechanical polish were finally polished using 0.01%  $\text{Br}_2$ -methanol solution.<sup>1</sup> A free etch in the same solution results in a good surface for reproducible Raman and ellipsometric measurements. The sample

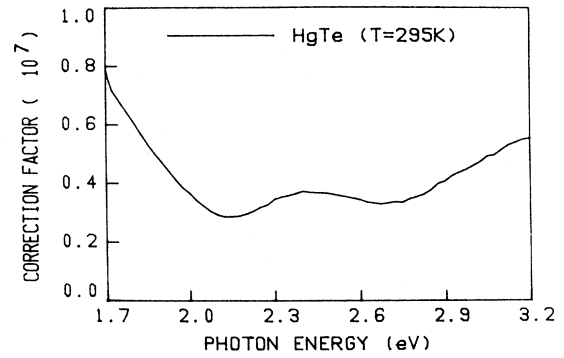


FIG. 2. Correction factor  $[T_L T_S / (\alpha_L + \alpha_S) \eta_L \eta_S]$  at room temperature based on ellipsometric measurements.

together with a (111) cut silicon wafer was mounted on the cold finger of a liquid-nitrogen ( $\text{LN}_2$ ) cryostat. Room-temperature measurements were rendered impossible as the sample surface was found to degrade due to laser heating with the formation of Te or  $\text{TeO}_2$  layers. All the experiments were performed at  $\text{LN}_2$  temperature. Raman spectra were recorded in a backscattering configuration with all the available lines of  $\text{Ar}^+$ ,  $\text{Kr}^+$ , and  $\text{He-Cd}^+$  lasers. A range below 2.2 eV was covered using  $\text{Ar}^+$ -laser-pumped Rhodamine-6G dye laser. Cylindrical focusing (spot size  $\sim 50 \mu\text{m} \times 1.2$  mm) with low laser power (maximum laser power  $\sim 100$  mW) has been used in order to avoid sample heating. The scattered light was analyzed with a double monochromator<sup>14</sup> and detected using a cooled ITT FW-130 photomultiplier in a photon counting mode. The data can be transferred to an IBM-PC for analysis.

We also simultaneously measured the Raman intensity of the  $522\text{-cm}^{-1}$  mode of Si in order to determine the absolute Raman susceptibility for HgTe with reference to Si. For Raman susceptibility of silicon we use an expression

$$a(\text{Si}) = 70 / (E_g - E)^{3/2} \text{ \AA}^2.$$

This expression gives a better fit over the range 1.8 to 3 eV for the various data found in literature.<sup>15,16</sup> The factor 70 itself has a large error bar (+15%). The other important factor required for obtaining  $|a_{\text{TO}}|^2$  for HgTe is the correction due to absorption and transmission and is given by  $T_S T_L / (\alpha_L + \alpha_S) \eta_L \eta_S$ . In Fig. 2 we show the variation of this factor as a function of energy. Intensity of the forbidden LO-phonon mode was measured from the (110) face also.

## V. RESULTS AND DISCUSSIONS

### A. TO phonon

In Fig. 3 we show the typical spectra obtained at three different laser wavelengths. As is clear from the figure the lowest frequency peak is quite close in frequency to the TO phonon. Therefore, we have used the least-squares fit to extract the intensity of the TO phonon. The origin of the lowest frequency peak is not very clear and

we do not discuss it here. The large intensity of the LO-phonon mode as one approaches the  $E_1$  gap is consistent with its being dominantly forbidden. We discuss this variation in Sec. VB. Using Eq. (1) and after taking care of various factors the obtained Raman susceptibility squared for the TO phonon is plotted as discrete points in Fig. 4.

For theoretical calculation of the Raman susceptibility using the expression given by Eq. (2), it is necessary that the functional dependence of amplitudes  $A^{E_1}$  and  $A^{E_1+\Delta_1}$  [Eq. (4)] on  $E_1$  be accurately known.<sup>2</sup> As is clear from Eq. (5) this implies that dependence of  $\mu_1^*$  on  $E_1$  be explicitly known. Even so its explicit inclusion for evaluating  $d\chi/dE_1$  depends upon the model used<sup>2</sup> to calculate the variation of  $\mu_1^*$  with phonon perturbation. If the phonon is assumed not to deform the electron bands,  $\mu_1^*$  in Eq. (5) can be treated as a constant independent of

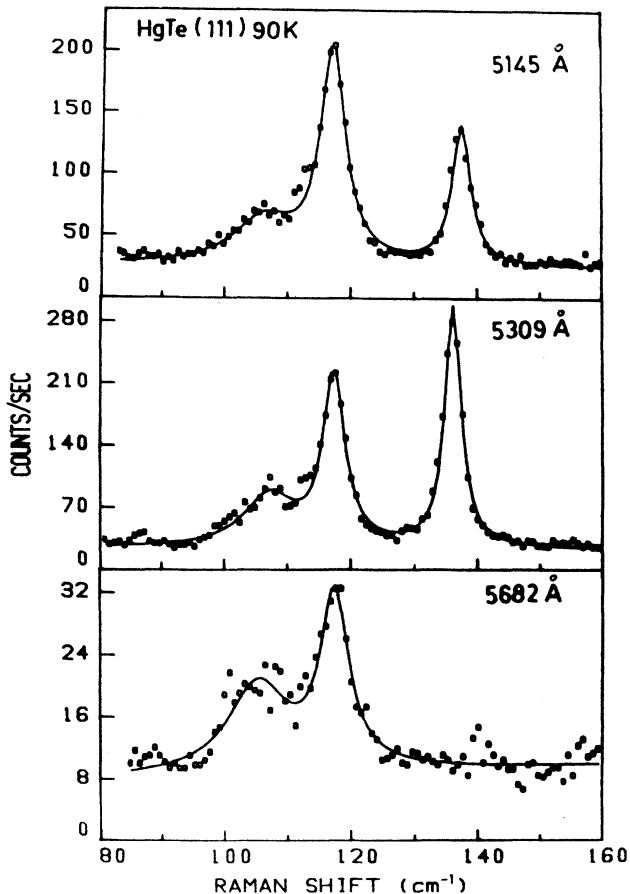


FIG. 3. Typical Raman spectra for HgTe(111) at 90 K with three different wavelengths. 100 mW of laser power was used for each run. Solid lines are least-squares-fit-curves. The modes at 117 and 137  $\text{cm}^{-1}$  are the TO and LO phonons, respectively. The low-frequency shoulder at around 100  $\text{cm}^{-1}$  is believed to arise from combination modes and its frequency decreases with temperature.

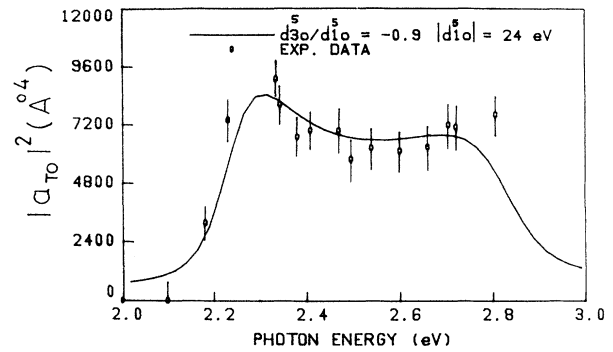


FIG. 4. Measured resonance in the Raman susceptibility of HgTe for the allowed-TO-phonon scattering at 90 K. The error bars are based on scatter in the data in repetitive runs. The solid circle corresponds to the data based on the temperature tuning of the gap. The solid curve is a calculation using Eq. (2) with  $|d_{30}^5|=20$  eV and  $|d_{10}^5|=24$  eV. The calculated curve has been shifted by about 0.1 eV to account for temperature hardening of the  $E_1$  gap as explained in the text.

$E_1$  for evaluating  $d\chi/dE_1$ . This is equivalent to taking  $\alpha=2$  as discussed by Cardona<sup>2</sup> in expanding  $d\chi/dE_1$  in terms of  $d\chi/dE$ . The extreme case where this dependence of  $\mu_1^*$  on energy is explicitly included corresponds to  $\alpha=1$ . The actual situation is generally between the two and depends upon the model used.

In order to fit our experimental data for the TO-phonon intensity variation we tried both possibilities. We find that it is not at all possible to fit the observed behavior (irrespective of the magnitude and sign of the ratio  $d_{30}^5/d_{10}^5$ ) using linear dependence of  $\mu_1^*$  on  $E_1$  ( $\alpha=1$ ). With the band deformation neglected ( $\mu_1^*$  independent of  $E_1$ , i.e.,  $\alpha=2$ ), we obtain a reasonable fit with  $d_{30}^5/d_{10}^5 = -0.9$  as shown in fig. 4.

Here we would like to emphasize that the constant  $C$  of Eq. (2) has not been treated as a parameter. It is the same as that used in Eq. (4b), i.e., the sloping contribution due to the  $E_2$  gap. We have, however, assumed that the deformation potential of the  $E_2$  gap is same as that for  $E_1$ . This term, however, makes insignificant change in the shape of the resonance curve in the region of interest. The solid line in Fig. 4 shows the calculated resonance curve with  $(d_{30}^5/d_{10}^5) = -0.9$ ;  $|d_{10}^5| = 24$  eV and  $|d_{30}^5| = 21.6$  eV. The calculated curve has been obtained using room-temperature susceptibility, a shift of around 0.1 eV has been incorporated to account for temperature hardening of gaps ( $dE_1/dT \sim 0.54 \times 10^{-3}$  eV/K,  $\Delta_1$ ,  $\Gamma_1$ , and  $\Gamma_2$  are more or less constant with temperature<sup>17,18</sup>).

It should be clear from Fig. 4 that the value of Raman susceptibility squared that we have obtained for HgTe is about a factor of 50 less than that for Ge and about a factor of 5 less as compared to InSb. Such a small value of  $|a_{TO}|^2$  coupled with small penetration depth makes the measurements difficult in HgTe. Notwithstanding the difficulties the results presented in Fig. 4 are an average of several sets of experiments. On this basis one can put an error bar of about 20% on the values of  $d_{10}$  and  $d_{30}$

that we have obtained. To some extent modeling of phonon-induced band deformation (choice of  $\alpha$  less than 2) may also affect the value of these deformation potentials. Nevertheless it is worthwhile pointing out here that large electron damping ( $\Gamma_1, \Gamma_2 \sim 0.1$  eV) in HgTe *vis-à-vis* other well studied diamond zinc blendes, results in small  $d\chi/dE_1$  (comparable to  $\chi$ ) and therefore the three-band contribution is comparable to two-band contribution. As a consequence the shape of the resonance curve is an extremely sensitive function of the ratio  $d_{30}^5/d_{10}^5$  and  $\alpha$ .

No theoretical calculations are available for the optical deformation potentials in HgTe. Therefore the only comparison that can be made is with other zinc-blende materials.<sup>2</sup> As has been mentioned earlier that InSb has similar energies  $E_1$  and  $E_1 + \Delta_1$ . Recently Menendez *et al.*<sup>8</sup> have obtained  $d_{10}^5 = -16$  eV and  $d_{30}^5 = 33$  eV, for InSb. In fact most of the tetrahedral semiconductors for which calculations have been performed have  $d_{10}^5$  values ranging from  $-10$  to  $-20$  eV,<sup>2,19</sup> and these are expected to be weakly dependent upon chemical constituents. In view of this the value of  $d_{10}^5$  obtained for HgTe is reasonable.

Theoretical values of  $d_{30}^5$ , however, are all around 40 eV.<sup>19</sup> This is borne out experimentally for Ge (46 eV),<sup>10</sup> GaAs (37 eV) (Ref. 2), and InSb (33 eV).<sup>8</sup> It is clear that the value of  $d_{30}^5$  obtained by us for HgTe is a factor of 3 less than that for other zinc-blende materials. Such a small value of  $d_{30}^5$  for HgTe can be explained if one recalls that  $d_{30}^5$  represents mixing of hh and lh valence bands.<sup>1,2</sup> Both these valence bands originate from a *p*-like atomic state in case of normal zinc-blende semiconductors. HgTe, however, has inverted band structure as a consequence of which the hh valence band originates from a *p*-like atomic state and the lh (lower) valence band originates from a *s*-like atomic state. Thus at the *L*-point one would expect the phonon to cause only a small mixing of these two states. We believe, therefore, that the small value of  $d_{30}^5$  that we have obtained for HgTe is a direct consequence of inverted band structure of HgTe. Similar behavior should be expected in HgSe, which also has inverted band structure.

Preliminary data on mixed system  $\text{Hg}_{1-x}\text{Cd}_x\text{Te}_1$  ( $x = 0.27$ ), reported recently by Compaan *et al.*<sup>20</sup> show a resonance behavior qualitatively similar to that obtained by us.

### B. Forbidden LO scattering

The selection rules for dipole-allowed LO-phonon scattering<sup>2</sup> are determined by the Raman tensor  $\mathcal{R}_{ij} = a_{\text{LO}}(1 - \delta_{ij})$  which is similar to that given earlier for TO phonons. However, the transition susceptibility corresponding to Raman scattering for LO phonon has, in addition to deformation-potential term, contribution arising from Fröhlich interaction of electrons with the longitudinal macroscopic electric field associated with polar lattice vibration. This is termed as the electro-optic part of the Raman tensor. Further, it can be shown that for allowed LO-phonon scattering in the vanishing  $q$  limit only the three-band terms need be considered.<sup>21</sup> For the present discussion in HgTe, these interband terms corre-

spond to intermediate electronic states which have holes in the valence bands  $|hh\rangle$  and  $|lh\rangle$  mediated via Fröhlich interaction. The frequency dispersion of this resonant part may be expected to be qualitatively similar to that of the three-band contribution to the atomic displacement tensor.<sup>21</sup>

It follows from the form of the Raman tensor that the allowed-LO-phonon intensity in the backscattering geometry vanishes corresponding to the (110) face of the crystal. However, if there is an additional vector perturbation perpendicular to the surface, e.g., electric field or finite wave vector  $q$  of the phonon, Raman intensity of the LO mode can be nonzero. This is usually termed as "forbidden" scattering.<sup>2,21</sup> Similarly, the presence of impurities can provide an additional scattering mechanism. In this case since the phonon wave vector  $q$  need not be conserved, processes involving  $q$  vectors which satisfy the "double resonance" condition are favored.<sup>22</sup> Therefore, for impurity-induced Fröhlich Raman scattering, 1LO and 2LO intensities can become of comparable magnitude. On the other hand, for an intrinsic process where  $q$  for 1LO scattering is small (limited by a photon wave vector) 2LO phonon intensity dominates since phonons of arbitrary wave vectors can take part in the scattering process.

Our measurements in HgTe for the forbidden LO-phonon intensity from the (110) and (111) (Ref. 23) faces are presented in Fig. 5. The intensities have been scaled by TO intensities. Consequently corrections in the cross section arising from the changing penetration depth of laser light in the sample with incident photon energy and spectrometer throughput variation are avoided.

It may be mentioned here that we find the 2LO intensity for HgTe near the  $E_1$  gap less than 1LO intensity.

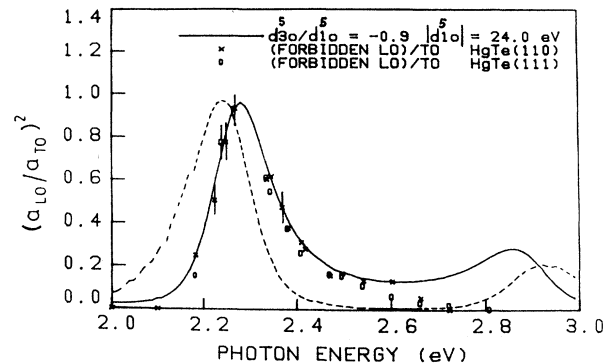


FIG. 5. The experimental data ( $\times, \circ$ ) on the forbidden-LO-phonon intensity scaled by TO-phonon intensity are plotted along with calculated curves. The points with error bars have been obtained by temperature tuning of the bands gap. The correction for temperature variation of the depletion region has been applied with reference to the data taken in the green region. The dashed line corresponds to  $d^2\chi/dE_1^2$ . The solid line is obtained by adding three-band contribution suitably and after shifting the curve by 0.04 eV (in addition to temperature hardening of the  $E_1$  gap) towards higher energy to yield an overall agreement with the experimental result.

This suggests dominance of impurity-induced scattering as described earlier. This is not unexpected as a large number of Hg vacancies, which exist near the surface, act as impurities.

For comparison of experimental data with theoretical calculations, we note that the dominant contribution to the Raman tensor is expected from two-band effects. This is given<sup>2</sup> by  $d^2\chi/dE_1^2$  and is shown by the dashed curve in Fig. 5. It has been evaluated using the expressions for  $\chi$  given in Eq. (4) and the parameters as determined from fitting to TO cross section. It is seen that the experimental forbidden-LO-phonon intensity has a comparatively gradual fall in the region  $E_1$  and  $E_1 + \Delta_1$ . This can be attributed to three-band contributions. The relative importance of three-band terms *vis-à-vis* two-band terms in the cross section can be expressed by the ratio  $(\Gamma_1/\Delta_1)^2$ . In HgTe this ratio is higher by an order of magnitude compared to InSb. The three-band contributions to the electro-optic term of the Raman tensor for the forbidden LO phonon can be related to the derivative of  $(\chi^{E_1} - \chi^{E_1 + \Delta_1})/\Delta_1$ . The solid curve in Fig. 5 is obtained after adding both the two-band and three-band contributions suitably to provide a qualitative agreement with the experimental data. The calculated curve is shifted by 0.04 eV towards higher energies to give a remark-

able agreement with the observed behavior in the  $E_1$  region. The energy shift can partially be accounted for by the dominance of outgoing resonance (occurring at  $E_1 + \hbar\omega_{LO}$ ) (Ref. 15) in impurity-induced scattering and partially because under the "double resonance" condition involving finite  $q$ , the peak position is shifted to high energy.<sup>24</sup>

## VI. CONCLUSIONS

We have shown that three-band terms play an important role in determining the shape of resonance curves for both the TO and forbidden LO mode near  $E_1$  and  $E_1 + \Delta_1$  gaps. The behavior is different from that observed in other narrow-gap semiconductors such as InSb. This is attributed to the large electron damping parameter associated with the  $E_1$  and  $E_1 + \Delta_1$  gaps in HgTe.

## ACKNOWLEDGMENTS

The authors are thankful to Professor A. K. Ramdas of Purdue University, U.S.A. for providing the mercury telluride sample. They are also grateful to Shri S. V. Rajarshi of Department of Physics, Poona University, for his help in ellipsometric measurements.

- 
- <sup>1</sup>W. Richter, in *Solid State Physics*, Vol. 78 of *Springer Tracts in Modern Physics*, edited by G. Höhler (Springer, Berlin, 1976), p. 121 and references therein.
- <sup>2</sup>M. Cardona, in *Light Scattering in Solids II*, Vol. 50 of *Topics in Applied Physics*, edited by M. Cardona and G. Guntherodt (Springer, Berlin, 1982), p. 19.
- <sup>3</sup>R. Dornhaus and G. Nimtz, in *Narrow Gap Semiconductors*, Vol. 98 of *Springer Tracts in Modern Physics*, edited by G. Höhler (Springer, Berlin, 1980).
- <sup>4</sup>A. Mooradian and T. C. Harman, in *The Physics of Semimetals and Narrow-Gap Semiconductors*, edited by D. L. Carter and R. T. Bate (Pergamon, Oxford, 1973).
- <sup>5</sup>P. M. Amiritharaj, K. K. Tiong, P. Parayanthal, and F. H. Polak, *J. Vac. Sci. Technol.* **A3**, 226 (1985).
- <sup>6</sup>K. Kumazaki and M. Cardona, *Mem. Hokkaido Inst. Technol.* **14**, 201 (1986).
- <sup>7</sup>L. Viña, C. Umbach, M. Cardona, and L. Vodopyanov, *Phys. Rev.* **B29**, 6752 (1984).
- <sup>8</sup>J. Menendez, L. Viña, M. Cardona, and E. Anastassakis, *Phys. Rev.* **B32**, 3966 (1985).
- <sup>9</sup>M. Cardona, *Modulation Spectroscopy* (Academic, New York, 1969).
- <sup>10</sup>A. K. Sood, G. Contreras, and M. Cardona, *Phys. Rev.* **B31**, 3760 (1985).
- <sup>11</sup>M. Cardona, in *Atomic Structure and Properties of Solids*, edited by E. Burstein (Academic, New York, 1972), p. 514.
- <sup>12</sup>W. Szymanska in *Proceedings of the Third International Conference on the Physics of Narrow Gap Semiconductors* (PWN—World Scientific, Warsaw, Poland, 1972).
- <sup>13</sup>M. V. Klein, in *Light Scattering in Solids*, Vol. 8 of *Topics in Applied Physics*, edited by M. Cardona (Springer, Berlin, 1975).
- <sup>14</sup>A. P. Roy and M. L. Bansal, *Indian J. Pure Appl. Phys.* **26**, 218 (1988), and references therein.
- <sup>15</sup>A. Compaan and H. J. Trodahl, *Phys. Rev. B* **29** 793 (1984).
- <sup>16</sup>M. Grimsditch and M. Cardona, *Phys. Status Solidi B* **102**, 155 (1980).
- <sup>17</sup>*Semiconductors: Physics of II-VI and I-VII Compounds, Semimagnetic Semiconductors*, Vol. III/17B of *Landolt Börnstein New Series*, edited by O. Madelung (Springer, New York, 1982).
- <sup>18</sup>A. Rodzik and A. Kisiel, *J. Phys. C* **16**, 203 (1983).
- <sup>19</sup>W. Potz and P. Vogl *Phys. Rev. B* **24**, 2025 (1981).
- <sup>20</sup>A. Compaan, B. Aggarwal, R. C. Bownan, Jr., and D. E. Cooper (unpublished).
- <sup>21</sup>A. Pinczuk and E. Burstein, in *Light Scattering in Solids*, Vol. 8 of *Topics in Applied Physics*, edited by M. Cardona (Springer, Berlin, 1975).
- <sup>22</sup>R. M. Martin, *Phys. Rev. B* **10**, 2620 (1974).
- <sup>23</sup>LO-phonon Raman scattering from the (111) face contains both allowed as well as dipole-forbidden contributions. However, measurement of LO-phonon intensity from the (100) face in diagonal and off-diagonal configurations indicates that the allowed-LO-phonon intensity is only 10% of forbidden-LO-phonon intensity in the neighborhood of the  $E_1$  critical point.
- <sup>24</sup>P. Y. Yu and Y. R. Shen, *Phys. Rev. Lett* **29**, 468 (1972).